JOURNAL OF SOLID STATE CHEMISTRY 6, 21–41 (1973)

Thermodynamic Relations Among Olivine, Spinel, and Phenacite Structures in Silicates and Germanates: I. Volume Relations and the Systems $NiO–MgO–GeO_2$ and $CoO–MgO–GeO_2$

A. NAVROTSKY

Department of Chemistry, Arizona State University, Tempe, Arizona 85281

Received February 22, 1972

An experimental approach is outlined to systematically obtain free energy differences among olivine, spinel, and phenacite forms of silicates and germanates from the thermodynamics of terminal solid solutions in ternary systems. This is applied to the ternary systems $NiO–MgO–GeO_2$ and $CoO–MgO–GeO_2$ at 1200°C in air and to the system $NiO–MgO–GeO_2$ at 800°C and 0.57 kbar water pressure. From the location of conjugation lines, activity–composition relations along each orthogermanate join are calculated. The free energies of transformation from the olivine to the spinel structure at 1200°C are estimated to be +1.6, −3.5, and −8.2 kcal/mole for Mg_2GeO_4, Co_2GeO_4, and Ni_2GeO_4, respectively.

Volume changes for the spinel–olivine and olivine–phenacite transitions are estimated for the silicates and germanates of Mg, Mn, Fe, Co, Ni, and Zn.

Introduction

Structural analogies and similarities among compounds of Si^{4+} and Ge^{4+} have long been recognized (*1*), and the germanate analogs of many rock-forming silicates often require less extreme temperature and pressure conditions for their formation than do the silicates. The use of germanates as model systems for the corresponding silicates has been pursued with enthusiasm (*1*, *2*), although recent studies have tended to emphasize differences in detail and to caution against too simple extrapolations (*3*, *4*, *24*). Nevertheless, systematic crystal chemistry and thermodynamics have much to gain by exploring and comparing the effects on structure and stability of cation substitution, both of divalent cations and of tetravalent Ge and Si.

To focus attention on the stoichiometry AB_2O_4, a hypothetical generalized phase diagram is shown in Fig. 1, drawn to be consistent with observed phase relations in real germanate and silicate systems. Portions of this diagram, shown as dashed rectangles, correspond to experimentally attainable equilibrium pressures (0–125 kbar) and temperatures (500–1500°C) for the specific compounds indicated. Three major structural types (phenacite, olivine, and spinel) occur in these systems. Least dense is the phenacite structure, based on a hexagonal array of oxide ions and tetrahedral coordination for both cations. Zn_2GeO_4 and Zn_2SiO_4 crystallize as phenacites at atmospheric pressure; the former transforms to a spinel at high pressure (*5*, *6*), the latter apparently exhibits a sequence of high pressure transitions to complex and possibly nonstoichiometric phases (*4*, *6*). The olivine structure, based on a hexagonal and almost closed-packed oxygen array, with tetrahedral coordination for Si or Ge, and octahedral coordination for the divalent ions, is the familiar atmospheric pressure structure for the silicates Mg_2SiO_4, Mn_2SiO_4, Fe_2SiO_4, Co_2SiO_4, and Ni_2SiO_4 and also for Mn_2GeO_4 and the high temperature form of Mg_2GeO_4 (*7*). The spinel structure, based on a cubic close packed array of oxide ions, with octahedral coordination for two cations, and tetrahedral coordination for one cation per AB_2O_4 formula unit, is the structure at atmospheric pressure of Fe_2GeO_4, Co_2GeO_4, Ni_2GeO_4, and the low temperature modification of Mg_2GeO_4 (*7*). The transition olivine–spinel has been observed at high pressure in Fe_2SiO_4,

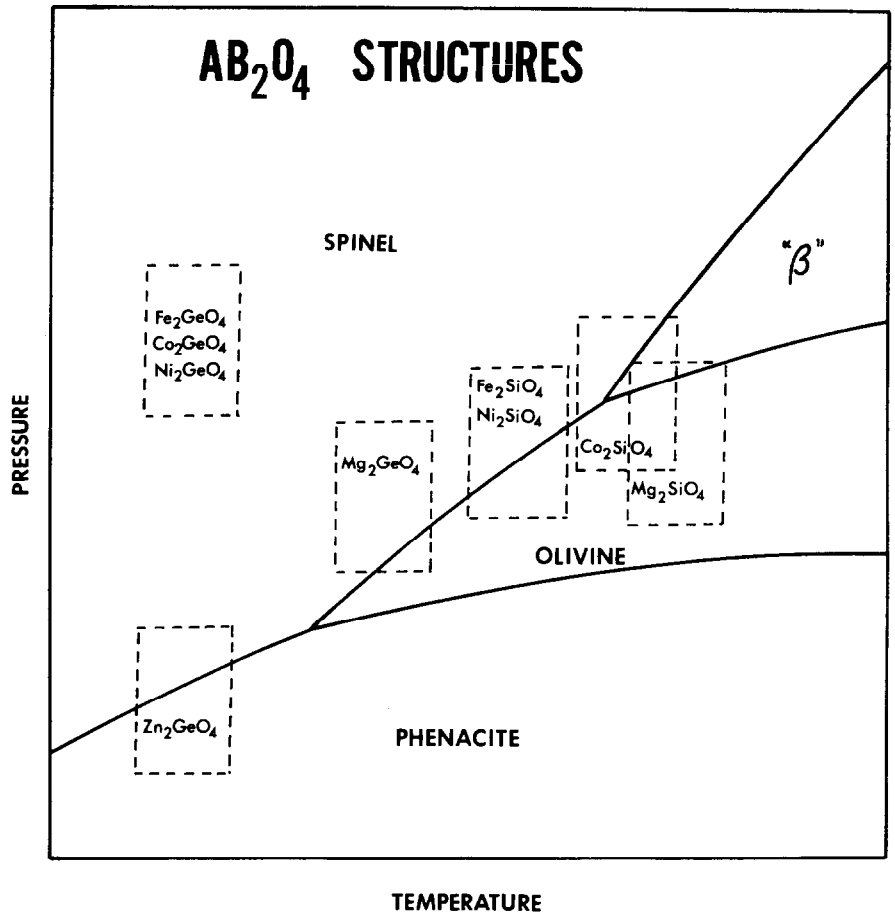

FIG. 1. Hypothetical P, T phase diagram for the stoichiometry AB_2O_4, showing possible relation among phenacite, olivine, spinel, and modified spinel structures.

Co_2SiO_4, and Ni_2SiO_4, and its occurrence in the natural system forsterite–fayalite (Mg_2SiO_4–Fe_2SiO_4) at depths of about 400 km in the earth's upper mantle is an exciting geological possibility (*2*, *7*). Recently, another structure type, the so-called "modified spinel" or "β", has been discovered for Co_2SiO_4 (*8*) and Mn_2SiO_4 (*9*), and seems to be the probable stable high-pressure, high-temperature structure in Mg_2SiO_4 (*10*) and Zn_2SiO_4 (*4*) as well. Since this modified spinel structure does not occur in Fe_2SiO_4, the forsterite–fayalite pseudobinary phase diagram at high pressure is probably more complex than initially supposed (*11*). The existence of the triple point, olivine–spinel–modified spinel, appears well-established in Co_2SiO_4 (*9*) and is the basis for the high-pressure portion of Fig. 1.

To quantitatively explain and predict the relative stabilities of these structure types as functions of temperature, pressure, and composition is certainly one of the goals of crystal chemistry. *A priori* predictions on theoretical grounds are generally not feasible for several reasons. First, the quantitative calculation of lattice energies, especially for low symmetry structures such as olivine, phenacite, and modified spinel, and particularly when these contain transition metal ions, cannot be done with sufficient accuracy to allow the calculated energy differences between these structures (on the order of 1% of the total lattice energy) to be meaningful. Second, the stability of a phase at a given constant temperature and pressure is determined by its Gibbs free energy, rather than by its lattice energy alone, and the theoretical calculation of the absolute entropy of such a complex solid would be an even more formidable task. Last, the possibility of substantial disorder, particularly in the cation distribution in the spinel structure, is a further complication.

Qualitative rationalizations of the relative stabilities of these structures has been more successful. Kamb (*11*) has offered an explanation of the olivine–spinel stability relations on the basis of Pauling's rules of edge sharing of coordination polyhedra. Reinen (*12*) has shown experimentally that the ligand field-splitting parameter Δ is greater for the octahedral site in spinel than for either octahedral site in olivine, and has attributed the decreasing stability of the spinel structure in the sequence Ni, Co ~ Fe, Mg, partly to this factor. The role of ligand field effects in the olivine–spinel transition has also been discussed more recently by Syono (*13*). The occurrence of the phenacite structure for the zinc germanate and silicate is generally explained by the preference of Zn^{2+} for tetrahedral coordination which results from its d^{10} electronic configuration and a tendency toward covalent bonding (*14*).

The Present Investigation

To transform such qualitative arguments into a more quantitative empirical theory of the stabilities of different structure types for the stoichiometry AB_2O_4, experimental thermodynamic data for these different structures for each stoichiometry would be very useful. The thermodynamics of formation from the oxides of the silicates and germanates which are stable at atmospheric pressure have been fairly well studied (except for the free energies of formation of the germanates) (*15*). The thermodynamics of the olivine–spinel transition has been quite thoroughly charted for those silicates in which the spinel is an accessible high pressure form (*9*, *10*, *16*, *17*). There ΔV can be obtained from crystallographic data, and ΔG, ΔH, and ΔS from the P, T of transformation and the slope of the phase boundary, $\partial P/\partial T$. However, one could also ask "How much less stable is the olivine form of Co_2GeO_4 than the spinel, or Mg_2SiO_4 phenacite than olivine?" Such data, though essential to a general picture of stability relations, cannot be gotten by direct study because the higher energy modifications would be metastable (monotropic) at all real P, T.

It is the aim of this series of papers to provide systematic data of this sort, through the study of the thermodynamics of extensive terminal solid solutions among two AB_2O_4 compounds of different structures. This can yield estimates of the free energies of transformation of each compound to the other form. A similar approach was applied first by Ringwood (*18*) to the system Mg_2SiO_4–Ni_2GeO_4 to provide an initial estimate of the free energy of transformation of forsterite to the spinel structure. A more precise value of this ΔG was later obtained by extrapolation of the pressure dependence of spinel–olivine phase boundaries in the system Fe_2SiO_4–Mg_2SiO_4 (*10*, *16*). In a series of papers, Muan and coworkers (*19*) have successfully obtained consistent free energies of formation of orthosilicate end members and activity–composition relations in their solid solutions from the study of subsolidus phase relations and the direction of conjugation lines in ternary systems of the type AO–BO–SiO_2. Recently, the determination of activity–composition relations in the systems CuO–CoO (*20*), CoO–ZnO and NiO–ZnO (*21*), and MgO–ZnO (*22*) has permitted the calculation of the free energies of transformation of CuO from the tenorite to the rocksalt structure, and of MgO, CoO, and NiO and ZnO from the rocksalt to the zincite structure.

A similar approach is particularly applicable to the germanates, since one can select pairs of end members such that their pseudobinary orthogermanate join exhibits olivine + spinel, olivine + phenacite, or spinel + phenacite structures at atmospheric pressure and a given temperature. By experimentally studying isothermal sections of the appropriate ternary systems AO–BO–GeO_2, the present work seeks to provide both approximate values of the free energies of formation of stable compounds and values of the free energies of transformation of these to the other metastable structures. These experimental studies can be classified according to the germanate structures involved: (1) olivine–spinel: the systems CoO–MgO–GeO_2, NiO–MgO–GeO_2 and "FeO"–MgO–GeO_2; (2) spinel–phenacite: the systems CoO–ZnO–GeO_2 and NiO–ZnO–GeO_2; (3) spinel–olivine–phenacite: the system MgO–ZnO–GeO_2 (because of dimorphism of Mg_2GeO_4); and (4) olivine–spinel plus two structures at the metagermanate composition; the system CuO–MgO–GeO_2.

Molar Volumes of Silicates and Germanates of the Olivine, Spinel, and Phenacite Structures

One can obtain the unit-cell dimensions of a real or hypothetical structural modification of a compound by direct measurement, extrapolation from the cell dimensions of a partial solid solution series, or estimation based on ionic radius considerations or similar reasoning.

TABLE I

CRYSTALLOGRAPHIC DATA FOR REAL AND HYPOTHETICAL SILICATES AND GERMANATES OF THE SPINEL, OLIVINE, AND PHENACITE STRUCTURES

	Spinel			Olivine						Phenacite				
	a_0 (Å)	V (A³)[a]	V (cm³/mole)[b]	a (Å)	b (Å)	c (Å)	V (A³)[a]	$\sqrt[3]{V}$ (Å)	V (cm³/mole)[b]	a (Å)	c (Å)	V (A³)[a]	$\sqrt[3]{V}$ (Å)	V (cm³/mole)[b]
Mg_2SiO_4	8.07[d]	525.6	39.58	4.76[c]	10.20	5.99	581.6	8.35	43.79				(8.86)[e]	(52.44)
Mn_2SiO_4				4.87[c]	10.64	6.23	645.6	8.63	48.61					
Fe_2SiO_4	8.234[c]	558.3	42.04	4.81[c]	10.61	6.17	629.8	8.51	46.39					
Co_2SiO_4	8.138[c]	538.9	40.58	4.78[c]	10.30	6.00	590.8	8.40	44.56	14.00[d]	9.35	706.3	8.90	53.18
Ni_2SiO_4	8.043[c]	520.3	39.18	4.71[c]	10.19	5.925	568.6	8.25	42.51					
Zn_2SiO_4	8.18[e]	547	41.19	4.79[d]	10.3	6.02	594	8.41	44.73	13.934[c]	9.307	696.4	8.86	52.44
Cd_2SiO_4														
Ca_2SiO_4				5.06[c]	11.28	6.78	774	9.18	58.28					
Be_2SiO_4										12.42[c]	8.24	547.3	8.18	41.19
Mg_2GeO_4	8.255[c]	562.5	42.35	4.915[c]	10.295	6.020	609.2	8.48	45.87	14.18_5[d]	9.51	737.4	9.03	55.31
Mn_2GeO_4				5.04[c]	10.7	6.26	675	8.79	50.82					
Fe_2GeO_4	8.411[c]	594.9	44.80				649	8.66[e]	48.87					
Co_2GeO_4	8.317[c]	575.3	43.32				627	8.56[e]	47.21				(9.07)[e]	(56.21)
Ni_2GeO_4	8.221[c]	555.5	41.83				597	8.42[e]	44.95					
Zn_2GeO_4	8.350[c]	582.2	43.84				629	8.57[e]	47.36	14.231[c]	9.530	743.7	9.06	56.00
Cd_2GeO_4				5.20[c]	11.13	6.57	761	9.13	57.30					
Ca_2GeO_4				5 14[c]	11.55	6.88	817	9.35	61.52					
Be_2GeO_4										12.756[c]	8.425	588.5	8.38	44.32

[a] For $(AB_2O_4)_8$, as in spinel unit-cell.
[b] For AB_2O_4.
[c] Measured on actual phase.
[d] Extrapolated from extensive solid solutions.
[e] Estimated from Fig. 3, this work.

Crystallographic parameters obtained by the first method for those compounds that can be synthesized at atmospheric or high pressure are listed in Table I.

The second method is useful when the modification in question cannot be obtained in its pure state, but a substantial mole fraction of that component (~50%) can be incorporated into a solid solution possessing the desired structure. Such extrapolated values, taken from the literature, are included in Table I.

As part of the present work, we have synthesized some compositions in the rather extensive phenacite field of the systems Zn_2GeO_4–Mg_2GeO_4 and Zn_2SiO_4–Co_2SiO_4. The variation of their lattice parameters with composition is shown in Fig. 2. Extrapolation to the zinc-free end gives for Mg_2GeO_4 (ph), $a = 14.18_5$ Å and $c = 9.51$ Å, while for Co_2SiO_4 (ph), $a = 14.00$ Å and $c = 9.35$ Å.

However, solid solution formation is not extensive enough to permit the evaluation of lattice constants for the olivine forms of Fe_2GeO_4, Co_2GeO_4, and Ni_2GeO_4, nor for the phenacite forms of most other silicates and germanates. The following observations offer a means to this end. Figure 3 plots the cube root of the volume of a unit cell containing 8 M_2GeO_4 formula-units versus the same quantity for the silicate of the same divalent cation, when both silicate and germanate crystallize in the same structure. This quantity $V^{1/3}$ is chosen so that it is simply the cubic lattice parameter for the spinel structure, while for the other structures it is the cell edge of a cube of volume equal to the actual $(AB_2O_4)_8$ cell volume. For nine isostructural silicate–germanate pairs the points fall very close to a straight line. A least-squares fit of the data gives:

$$V^{1/3}_{M_2GeO_4} = 1.00\ V^{1/3}_{M_2SiO_4} + 0.165. \qquad (1)$$

Note that the same linear relation holds for all three structures, olivine, spinel, and phenacite. Thus, the substitution of Ge^{4+} and Si^{4+}, with the structure and the divalent cation kept constant, results in the same expansion of equivalent cubic cell edge (though not necessarily the same relative expansion of each lattice parameter) in all these cases. This constancy reflects the essentially constant ionic radii of Si^{4+} and of Ge^{4+} in tetrahedral coordination in these compounds, and the additive constant in Eq. (1) is fortuitously close to the difference in the two ionic radii: $r_{Ge^{4+}} - r_{Si^{4+}} = 0.48 - 0.34 = 0.14$ Å (*23*). Obviously a different choice of unit-cell volume, such as that for 1 AB_2O_4 formula unit instead of for 8, would result in a different value for that constant.

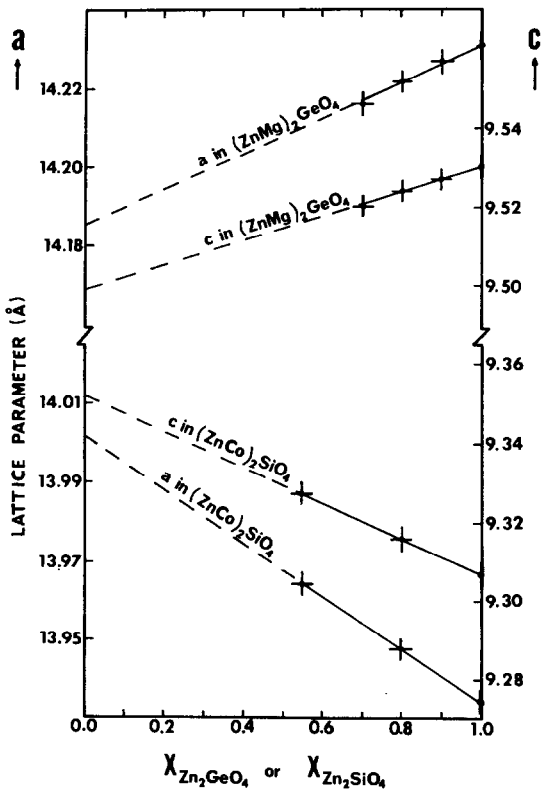

FIG. 2. Measured lattice parameters for phenacite phases in systems Zn_2GeO_4–Mg_2GeO_4 and Zn_2SiO_4–Co_2SiO_4. Samples synthesized at 1200 and 1300°C, respectively.

Figure 3 and Eq. (1) provide an easy way of estimating the unit-cell volumes of the olivine forms of Fe_2GeO_4, Co_2GeO_4 and Ni_2GeO_4, since the olivine forms of the corresponding silicates are well known. Similarly, since the spinel form of Zn_2GeO_4 is known at high pressure, the lattice constant of the hypothetical spinel form of Zn_2SiO_4 can be calculated. Lastly, since solid solutions provide estimates for the lattice constants of Mg_2GeO_4 (ph), Co_2SiO_4 (ph), and Zn_2SiO_4 (ol), we can estimate the unit cell volumes of the corresponding Mg_2SiO_4 (ph), Co_2GeO_4 (ph), and Zn_2GeO_4 (ol). All these values have been included in Table I.

The volume changes (in cm^3/mole) for the olivine–spinel transition in the silicates and germanates are shown in Table II. It is seen that the volume changes, both on an absolute and on a relative basis, are really quite constant, averaging -3.75 cm^3/mole and -8.2%, respectively.

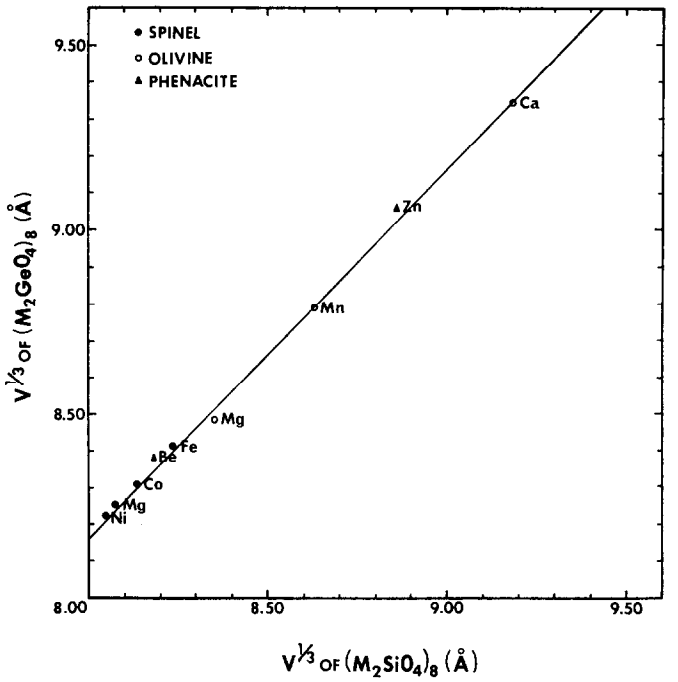

FIG. 3. Cube root of unit-cell volume containing 8 M_2GeO_4 formula units vs the same parameter for the silicate, with the structure and the divalent cation the same for each. Only those points for which the lattice constants are well known are shown.

TABLE II

VOLUME CHANGES OF PHASE TRANSITIONS, CALCULATED FROM DATA IN TABLE I

	Olivine → spinel	
Compound	ΔV (cm³/mole)	$\Delta V/V$ (%)
Mg_2SiO_4	−4.21	−9.6
Fe_2SiO_4	−4.35	−9.4
Co_2SiO_4	−3.98	−8.9
Ni_2SiO_4	−3.33	−7.8
Zn_2SiO_4	−3.54	−7.9
Mg_2GeO_4	−3.52	−7.7
Fe_2GeO_4	−4.07	−8.3
Co_2GeO_4	−3.89	−8.2
Ni_2GeO_4	−3.12	−6.9
Zn_2GeO_4	−3.52	−7.4
	av = −3.75 ± 0.4	av = −8.2
	Olivine → phenacite	
Compound	ΔV (cm³/mole)	$\Delta V/V$ (%)
Mg_2SiO_4	(+8.65)[a]	(+19.7)
Co_2SiO_4	+8.62	+19.3
Zn_2SiO_4	+7.71	+17.2
Mg_2GeO_4	+9.44	+20.6
Co_2GeO_4	(+9.0)[a]	(+19.1)
Zn_2GeO_4	(+8.64)[a]	+18.2
	av = +8.67 + 0.6	av = +19.0

[a] Value somewhat uncertain; see text.

Note that the calculations for the olivine–spinel transition in Zn_2SiO_4 involve the difference in unit cell volumes between two nonexistent compounds, since it is doubtful whether either Zn_2SiO_4 (ol) or Zn_2SiO_4 (sp) has any actual stability field. The fact that in reality other polymorphs appear more stable at high pressures in this system (as does β-Mg_2SiO_4 relative to Mg_2SiO_4 spinel) does not invalidate the reasoning used, although the extrapolations add to the uncertainties of the final values.

The volume data for the olivine–phenacite transition are also summarized in Table II. Solid solubility in the phenacite structure is not sufficient for either the germanate or the silicate of Fe or Ni to attempt any estimate of the crystallographic parameters of the pure-end members. The volume change of the olivine–phenacite transition in Zn_2SiO_4 can be estimated since the unit-cell dimensions of Zn_2SiO_4 (ol) have been found by extrapolation. Similarly, the data in Fig. 2 permit an estimate of the lattice constants of the phenacite forms of Co_2SiO_4 and Mg_2GeO_4. Lastly, Fig. 3 and Eq. (1) provide a means of approximating the unit-cell volumes of Zn_2GeO_4 (ol), Co_2GeO_4 (ph), and Mg_2SiO_4 (ph).

Although the values of ΔV and $\Delta V/V$ show a larger range for the olivine–phenacite transition than for the olivine–spinel transition, the data are adequately represented by an average volume change of $+8.7 \pm 0.6$ cm^3/mole or +19.0%.

The Systems CoO–MgO–GeO_2 and NiO–MgO–GeO_2: Previous Work

Although the existence and structures of ternary mixed metal oxides ($MgGeO_3$ (*25*), Mg_2GeO_4 (*7*, *25*, *28*), and $Mg_{28}Ge_{10}O_{48}$ (*25*, *26*) in the system MgO–GeO_2, $CoGeO_3$ (*27*), and Co_2GeO_4 (*28*) in CoO–GeO_2, and Ni_2GeO_4 (*28*) in NiO–GeO_2) are well known, relatively little work has been done on the details of binary and ternary phase diagrams in these systems. The system MgO–GeO_2 has been studied by Robbins and Levin (*25*) and by Dachille and Roy (*7*). Both the orthogermanate and metagermanate are compounds of high stability with congruent melting points of 1855 ± 30°C and 1700 ± 20°C. Mg_2GeO_4 is dimorphic at atmospheric pressure; the transition spinel → olivine occurs at 810°C (*7*). $MgGeO_3$ transforms from the orthoenstatite to the clinoenstatite structure at 1555°C. The magnesium-rich compound, initially thought to have the composition Mg_4GeO_6 ($X_{GeO_2} = 0.20$) (*25*) but actually having the composition $Mg_{28}Ge_{10}O_{48}$ ($X_{GeO_2} = 0.24$) (*26*) decomposes in the solid state to Mg_2GeO_4 and MgO at 1495 ± 10°C.

In the system CoO–GeO_2, $CoGeO_3$ exists in both orthorhombic low-temperature (orthoenstatite) and monoclinic (diopside) high-temperature forms (*29*) with the inversion at 1351°C. It melts congruently at 1377°C (*29*). The compound Co_2GeO_4 is known only as a spinel (*28*). In the system NiO–GeO_2, the spinel Ni_2GeO_4 is the only compound formed (*27*, *28*). Its melting point is above 1550°C, as evidenced by the work of Ringwood (*29*).

In the pseudobinary systems Co_2GeO_4–Mg_2GeO_4 and Ni_2GeO_4–Mg_2GeO_4 at 1200°C, Reinen (*12*) has found the solubility of Mg_2GeO_4 (olivine) in the spinel phase to be 70 and 55 mole%, respectively, while the solubility of Co_2GeO_4 in the olivine structure is 20 mole%, and of Ni_2GeO_4, 10 mole%. Within experimental error, the spinel solid solutions studied by Reinen follow Vegard's Law, and the extrapolated lattice constants for Mg_2GeO_4 (spinel) agree well with the lattice constants of the hydrothermally synthesized low-temperature spinel. Similar results were found by Ringwood at higher temperatures (*31*).

There has been some controversy in the literature concerning the cation distributions in germanate spinels. Early work (*28*) assumed these to be normal, $Ge[M_2]O_4$, but Dachille and Roy (*7*) suggested that their low temperature polymorph of Mg_2GeO_4 was an inverse spinel, $Mg[GeMg]O_4$, based on infrared absorption spectra. Datta and Roy (*32*) have also suggested, on the basis of X-ray intensity data on quenched powder samples, that Ni_2GeO_4 changes from a predominantly normal to a nearly random spinel at high temperatures. This conclusion has been questioned by Reinen (*12*). The presence of tetrahedral Ni^{2+} should be easily detectable by visible spectroscopy, but he has found no change in the spectra of heated Ni_2GeO_4 samples. Similarly, the visible spectra and regularly varying lattice parameters of the solid solutions between Mg_2GeO_4, and Co_2GeO_4 or Ni_2GeO_4 suggest that the concentration of divalent ions on tetrahedral sites is uniformly negligible and that Mg_2GeO_4 spinel has a normal cation distribution. These questions have a direct bearing on the thermodynamics of the solid solutions. For spinel systems in which large scale cation redistributions are known to occur, the activity composition relations can become quite complex, resulting, for example, in large negative deviations from ideality in the systems Co_3O_4–Fe_3O_4, Co_3O_4–Mn_3O_4, and Fe_3O_4–Mn_3O_4 (*33*), or in large positive deviations in the systems Co_2TiO_4–Zn_2TiO_4 and "Ni_2TiO_4"–Zn_2TiO_4 (*34*).

Experimental

Starting materials were reagent grade MgO, NiO, Co_3O_4, and hexagonal GeO_2. The MgO was ignited at 1050°C before use, while the other materials were ignited at 800°C. Samples of the desired compositions were weighed, ground under acetone, dried, pre-reacted in platinum crucibles in a muffle furnace at 1050°C, and ground again to a fine powder. Phase equilibrium runs in air were performed by the usual quenching techniques. Small portions of these prereacted samples were contained in open silver–palladium capsules and equilibrated in temperature controlled furnaces for 24–72 hr. Two furnaces were used, a vertical Kanthal wound furnace for temperatures below 1100°C, and a vertical "globar" rod furnace for higher temperatures. Temperature control, using a Pt–Pt10Rh control couple and commercial controllers, held the

measured furnace temperature constant to ±3°C during a run. Furnace temperature was measured by a second Pt–Pt10Rh thermocouple, periodically calibrated against a National Bureau of Standards standard thermocouple. The measuring thermocouple and the samples were carefully positioned next to each other in the hot spot of the furnace.

At the end of each run, the samples were quenched in air. Because of the small capsule size, the temperature of the samples dropped to below 100°C in several seconds. The sintered samples were then ground under acetone, and mounted on glass slides for phase identification. Because the grain size of the samples was generally too small for satisfactory microscopic study, X-ray diffraction proved the most useful identification technique. Powder patterns, using a Norelco diffractometer, filtered Cu$K\alpha$ radiation, and a scan speed of $2°(2\theta)$/min were routinely determined. This method could generally detect about 2% of a second phase in the sample.

Lattice parameters of the phases present were determined using the same diffractometer, an internal standard of either α-Al_2O_3 or NaCl, and a scan speed of $\frac{1}{4}°(2\theta)$/min. The compositions of one or both of two coexisting phases (conjugation lines) were calculated from their lattice constants after the variation of lattice constant with composition in each solid solution series had been determined.

The attainment of equilibrium in the "dry" runs were checked in two ways. Certain selected runs were equilibrated for much longer times (4–5 days) to make sure no further changes occurred. Selected compositions were prepared from different starting materials (unreacted oxides, mixtures of different binary end members) and equilibrated to give the same final phase assemblage. These tests suggested that there was no difficulty in attaining equilibrium in 48 hr at temperatures above 1000°C.

Hydrothermal runs on the system NiO–MgO–GeO_2 were performed as follows. Samples of about 150 mg each plus about 20 mg H_2O were sealed in 60Ag–40Pd capsules of 0.20 in. o.d. and about 1 in. in length. These were then placed, 3 or 4 capsules at a time, in a "stellite" hydrothermal bomb of $\frac{1}{2}$ in. i.d. The system was pressurized with water to 0.57 kbar, and placed in a vertical Kanthal furnace so the position of the samples corresponded to the furnace hot spot. Temperature was monitored by a chromel–alumel thermocouple external to the bomb and was controlled by a constant voltage transformer and variac. After the samples were brought to the desired P and T, the bomb was closed off from the rest of the pressurizing system and operated as a closed system for the remainder of the run. After 48–72 hr, the furnace was lifted from the pressure vessel, and a closely fitting head with copper coils circulating cold water was placed on the hot top of the bomb to cool the samples as rapidly as possible. Although not a true quench, this method brought the samples down to below 200°C in about 10 min. The samples were then removed and analyzed as before.

These runs were performed at 800 ± 5°C and 0.57 kbar in order to attain equilibrium between rocksalt and spinel phases at a temperature below the spinel–olivine transition in Mg_2GeO_4 and at a water pressure high enough to catalyze equilibration but low enough to make pressure effects almost negligible. A bomb holding several samples at a time was used to minimize the number of separate runs needed to get the conjugation lines, so that all samples would be exposed to nearly equal P, T conditions despite uncertainties introduced by the use of an external thermocouple.

Results

Subsolidus Phase Relations in Pseudobinary Systems Ni_2GeO_4–Mg_2GeO_4 and Co_2GeO_4–Mg_2GeO_4

The results of quenching experiments in air on samples along the orthogermanate join are shown in Fig. 4 for the nickel-containing and in Fig. 5 for the cobalt-containing systems. In both cases, a continuous spinel solid solution is formed below 810°C (*7*). A miscibility gap sets in when Mg_2GeO_4 transforms to the olivine structure, and the solubility of Ni_2GeO_4 and of Co_2GeO_4 in the olivine phase increases in a normal manner with increasing temperature. The boundary of the spinel phase shows more complex behavior. In both systems, the solubility of Mg_2GeO_4 in the spinel phase at first decreases with increasing temperature because of the decreasing stability of the spinel compared to the olivine at temperatures further above the spinel–olivine transition. Then, in the range 1100–1300°C, the decrease in solubility becomes much less pronounced in the nickel-containing system, while the phase boundary begins to slope

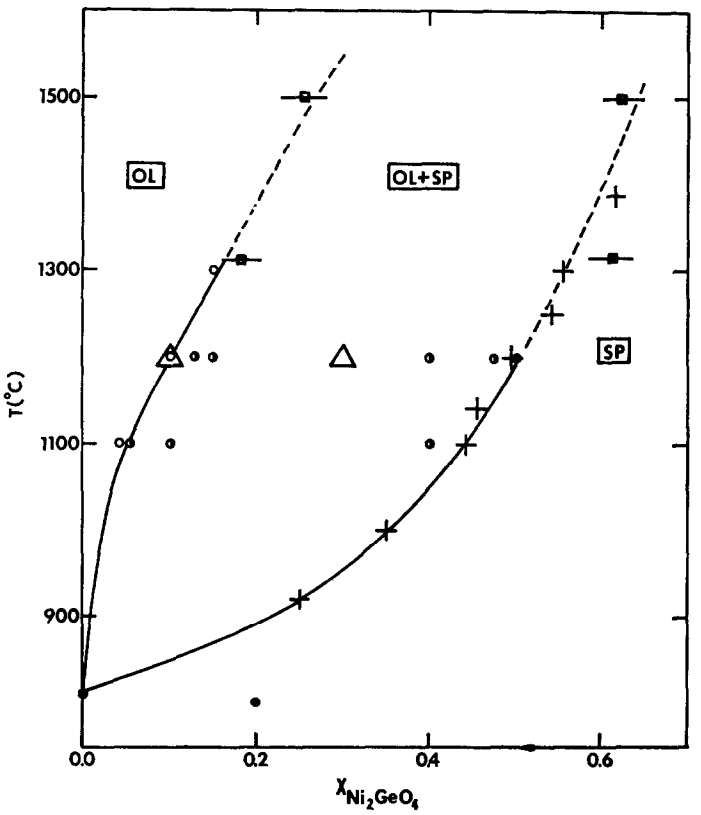

FIG. 4. The Ni_2GeO_4–Mg_2GeO_4 join in air. Filled circles: spinel; half filled circles: spinel plus olivine; open circles: olivine. Triangles: phase boundaries of Reinen (*9*); squares: phase boundaries of Ringwood (*8*, *10*). Olivine–spinel transition in pure Mg_2GeO_4 from Dachille and Roy (*2*).

toward increasing Mg_2GeO_4 content in the Co_2GeO_4–Mg_2GeO_4 system.

The limits of solubility at 1200°C in both systems are only in fair agreement with those reported by Reinen (*12*). An extrapolation to 1500°C of the phase boundaries in Ni_2GeO_4–Mg_2GeO_4 shows good agreement with the solubilities estimated by Ringwood (*30*). At temperatures near 1300°C, our boundaries in both systems also agree fairly well with those reported by Ringwood (*31*), although we report a somewhat larger solubility of Mg_2GeO_4 in the cobalt-containing spinel phase. One possible explanation for this discrepancy is that our samples were equilibrated for longer times (48–96 hr) than Ringwood's (3 hr) or Reinen's (5–20 hr).

In the Co_2GeO_4–Mg_2GeO_4 system, the two phase boundaries appear to approach each other at the highest temperatures studied here, making the two phase region (olivine and spinel) very narrow. Since the two structures are quite different, complete solid solubility between them is impossible. Therefore, it seems likely that some other phenomenon, probably melting, intervenes to terminate the two phase region at higher temperatures.

The smaller solubility of Ni_2GeO_4 than of Co_2GeO_4 in the olivine structure is indicative of the greater instability, relative to spinel, of the olivine structure for Ni_2GeO_4 than for Co_2GeO_4 (see below).

Isothermal Sections of Ternary Systems

The system NiO–MgO–GeO_2 at 1200°C in air is shown in Fig. 6. In addition to the continuous rocksalt (NiMg)O solid solution and spinel plus olivine on the orthogermanate join, the metagermanate of pyroxene (orthoenstatite) structure, takes up a small amount (~13 mole %) of $NiGeO_3$ in solid solution. The limited extent of the pyroxene solid solution is consistent with the nonexistence of $NiGeO_3$ as a pure phase under any pressure and temperature conditions. Al-

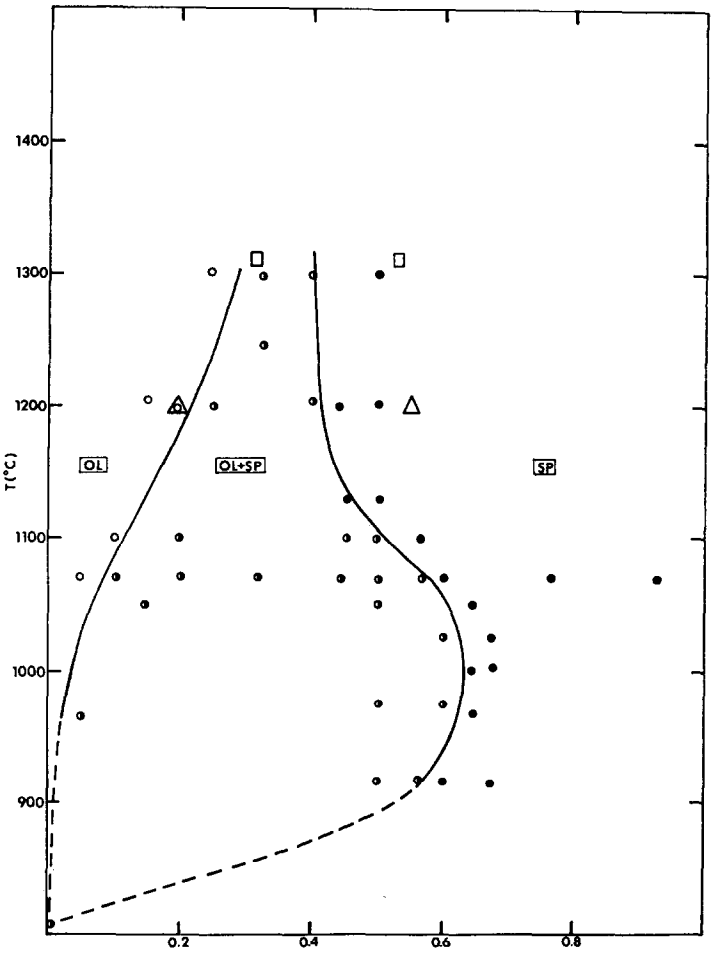

FIG. 5. The Co_2GeO_4–Mg_2GeO_4 join in air. Symbols same as in Fig. 4.

though the compound $Mg_{28}Ge_{10}O_{48}$ (*26*) exists in the MgO–GeO_2 system, a solid solution at that composition does not extend to any measurable distance into the ternary diagram, and the equilibrium between $(NiMg)_2GeO_4$ and (NiMg)O can be studied directly. Three-phase triangles and conjugation lines are shown. The spinel–rocksalt tie lines in and at the boundary of the two-phase region were established by lattice constant measurements on both phases. Since the melting point of hexagonal GeO_2 is 1116°C (*35*), the GeO_2-rich corner of the isothermal section contains a liquid phase, but this region of the phase diagram was not studied in the present work.

At 800°C and 0.57 kbar water pressure, the spinel solid solution in the system NiO–MgO–GeO_2 is continuous. Tie lines in the rocksalt plus spinel field, determined from the lattice parameters of both phases, are shown in Fig. 7. Again, the most MgO-rich germanate, $Mg_{28}Ge_{10}O_{48}$, was not found to extend into the ternary system.

The ternary system CoO–MgO–GeO_2 represents a rather different picture. The metagermanate join was confirmed to be a continuous pyroxene solid solution by direct synthesis of some intermediate compounds. The orthogermanate join consists of olivine and spinel, and the location of the olivine–spinel–pyroxene three-phase triangle was determined as shown in Fig. 8. Tie-lines in the spinel plus pyroxene two-phase region were determined through lattice parameter measurements on the spinel phase.

Attempts to prepare samples in the orthogermanate plus oxide field ($0 < X_{GeO_2} < 0.33$) resulted in dark red to black products showing

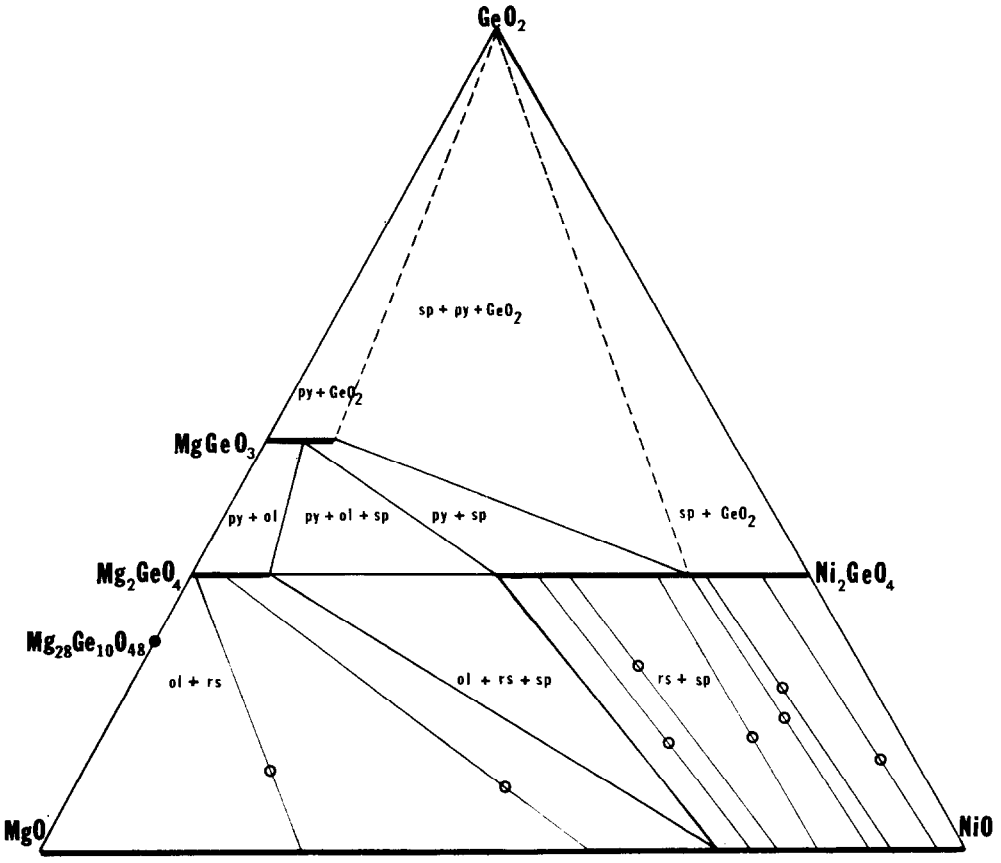

FIG. 6. The system NiO–MgO–GeO_2 in air at 1200°C. Open circles indicate compositions of samples used to find conjugation lines. Liquid present near GeO_2 corner.

complex X-ray diffractograms which were somewhat similar to all ratios of Co/Co + Mg. The composition $Co_{28}Ge_{10}O_{48}$ (assuming all cobalt is Co^{2+}), analogous to $Mg_{28}Ge_{10}O_{48}$ was prepared by heating an appropriate mixture of Co_3O_4 and GeO_2 in air at 1050°C. The product was black, slightly magnetic, and its powder X-ray diffraction pattern is shown in Table III. It is clearly not a mixture of the two cubic phases Co_2GeO_4 (spinel) and CoO (rocksalt). Microscopic examination of the material could detect small grains showing crystal faces that appeared to be of fairly low symmetry, as well as a minor amount of isotropic red crystals, presumably Co_2GeO_4.

Heating this material in air at 1200°C left it

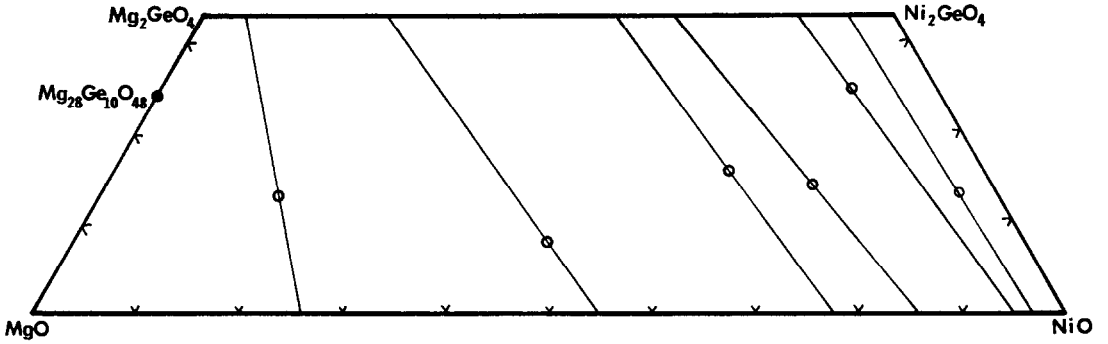

FIG. 7. The quadrilateral NiO–MgO–Ni_2GeO_4–Mg_2GeO_4 at 800°C and 0.57 kbar water pressure.

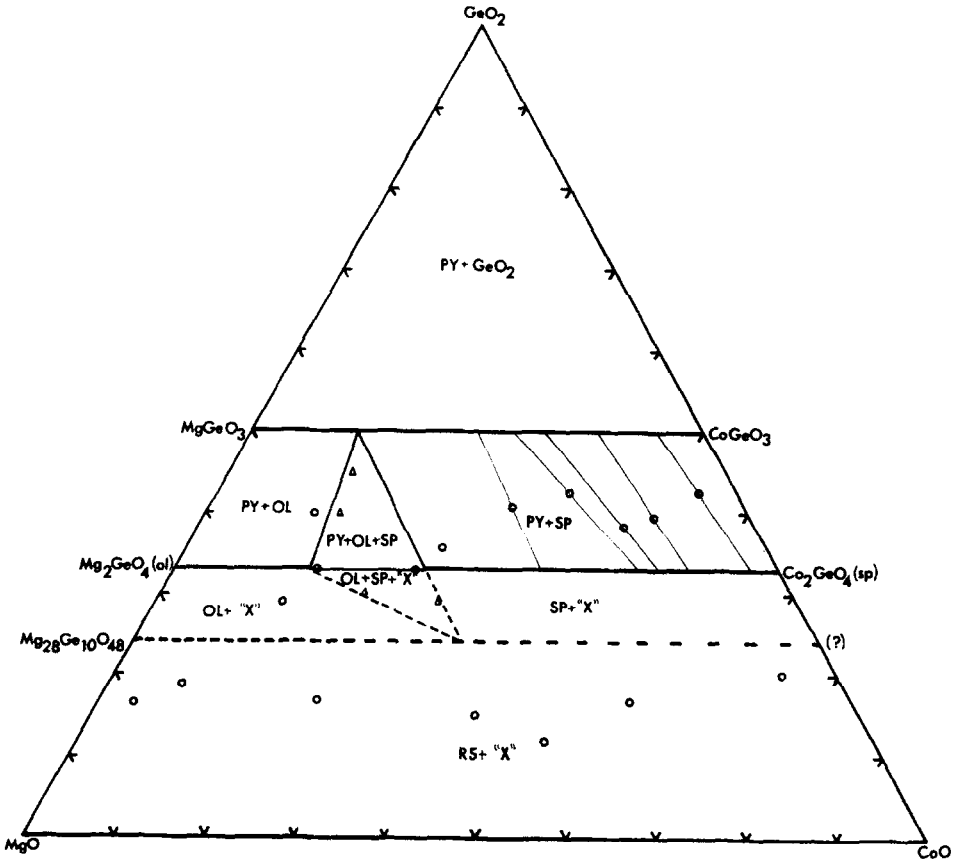

FIG. 8. The system CoO–MgO–GeO_2 in air at 1200°C. Open circles: two-phase; triangles: three-phase. Liquid present near GeO_2 corner.

apparently unchanged. Heating at 1040°C in pure CO_2 caused it to lighten in color to a dark reddish-brown, while its X-ray powder diffraction pattern showed no major changes in peak positions, but did show some possible shifts in relative intensities. Heating in a CO/CO_2 mixture at a P_{O_2} of $\sim 10^{-10}$ atm and 1040°C resulted in the loss of germanium (as Ge or GeO) and left a sample consisting almost entirely of CoO.

Work is in progress (R. B. Von Dreele of our department) on further characterizing this compound or series of compounds. For the purposes of the present study, the existence of a series of cobalt–magnesium germanates at or near $X_{GeO_2} = 0.24$ is established, and precludes the determination of conjugation lines between orthogermanate and rocksalt phases. This series may be a continuous solid solution between magnesium and cobalt end members, but may also be a considerably more complex group of possibly nonstoichiometric compounds. In Fig. 8, the as yet unexplored complexities of this region are shown schematically as a hatched line of some width extending from the known compound $Mg_{28}Ge_{10}O_{48}$ to its hypothetical cobalt analog.

Lattice Parameters

It is rather well established that the systems CoO–MgO and NiO–MgO follow Vegard's law rather closely and are indeed thermodynamically virtually ideal (*36–38*). Our measurements confirmed this fact, and our measured lattice constants for MgO, CoO, and NiO: 4.211 ± 0.001 Å, 4.261 ± 0.001 Å, and 4.176 ± 0.001 Å, respectively, agree well with previous values.

Our data for the spinel solid solutions are shown in Table IV. They agree well with the data of Reinen (*12*) and of Ringwood (*31*), and the extrapolated lattice parameter of Mg_2GeO_4 agrees with that of the hydrothermally synthesized phase (*7*).

TABLE III

POWDER X-RAY DIFFRACTION DATA FOR COMPOUND IN SYSTEM CoO–GeO_2 NEAR $X_{GeO_2} = 0.24$

$2\theta(CuK_\alpha)$	d	I/I_0
23.13	3.845	15
27.73	3.217	20
30.51	2.962	25
31.47	2.843	25
34.96	2.566	20
35.32	2.541	50
36.55	2.458	10
37.03	2.427	40
37.32	2.409	10
37.82	2.379	15
38.22	2.355	20
41.35	2.183	10
42.46	2.129	20
43.11	2.098	100
44.35	2.042	10
49.51	1.841	15
53.45	1.714	15
54.19	1.693	10
56.92	1.618	25
61.56	1.506	15
62.36	1.489	50
62.77	1.480	50

Lattice constants in the pyroxene solid solution series (CoMg)GeO_3 were calculated using 8–10 peaks in the $20° < 2\theta < 70°$ (CuK_α radiation) and a least-squares computer program. The results are shown in Table V.

Thermodynamic Calculations and Discussion

Activity–Composition Relations

In the system NiO–MgO–GeO_2, activity–composition relations along the orthogermanate join can be calculated from the conjugation lines between $(NiMg)_2GeO_4$ and (NiMg)O phases according to a method applied to oxide systems by Muan (*19*). For the equilibrium at constant temperature and pressure:

$$(NiO)_{ss} + (MgGe_{0.5}O_2)_{ss} = (MgO)_{ss} + (NiGe_{0.5}O_2)_{ss}, \quad (2)$$

one may write:

$$\log K = \log \frac{a_{MgO} X_{NiGe_{0.5}O_2}}{a_{NiO} X_{MgGe_{0.5}O_2}} + \log \gamma_{NiGe_{0.5}O_2} - \log \gamma_{MgGe_{0.5}O_2}. \quad (3)$$

TABLE IV

LATTICE CONSTANTS OF SPINEL PHASE IN SYSTEMS Ni_2GeO_4–Mg_2GeO_4 AND Co_2GeO_4–Mg_2GeO_4

$X_{Mg_2GeO_4}$	a_0 (Å) in Ni_2GeO_4–Mg_2GeO_4	a_0 (Å) in Co_2GeO_4–Mg_2GeO_4
0.00[a]	8.221	8.317
0.15[a]	8.226	8.308
0.30[a]	8.231	8.299
0.50[a]	8.237	8.286
0.80[b]	8.247	—
1.00[b]	8.255	—
1.00[c]	8.255	8.255

[a] Measured on products of "dry" runs, 1200°C, air.
[b] Measured on products of hydrothermal runs, 800°C, p.57 kbar.
[c] Extrapolated from 1200°C runs.

The first term on the right-hand side of Eq. (3) can be calculated if the conjugation lines between orthogermanate and rocksalt phases and the activity–composition relations in (NiMg)O are known. This term will be called $\log C$ and will vary with composition if the orthogermanate solid solutions deviate from ideality. Imposing the Gibbs–Duhem relations and the constancy of $\log K$, one can solve for the activity coefficients to get (*19*):

$$\log \gamma_{NiGe_{0.5}O_2} = -(1 - X)\log C - \int_1^X \log C \, dX, \quad (4)$$

and

$$\log \gamma_{MgGe_{0.5}O_2} = X \log C - \int_0^X \log C \, dX, \quad (5)$$

where $X = X_{NiGe_{0.5}O_2}$.

The system NiO–MgO has been found to be thermodynamically ideal at 1200°C (*37*), and to be virtually ideal from 840–1200°C (*38*) so that values of $\log C$ are readily calculated from our

TABLE V

LATTICE PARAMETERS AND UNIT CELL VOLUMES IN THE SYSTEM (CoMg)GeO_3

X_{CoGeO_3}	a (Å)	b (Å)	c (Å)	V (Å^3)
0.00	18.66 ± 0.01	8.95 ± 0.01	5.34 ± 0.01	891.8
0.29	18.73 ± 0 02	8.97 ± 0.02	5.34 ± 0.01	897.2
0.56	18.74 ± 0.02	8.97 ± 0.01	5.35 ± 0.01	899.3
0.76	18.78 ± 0.02	8.98 ± 0.02	5.34 ± 0.01	900.5
1.00	18.80 ± 0.02	8.99 ± 0.01	5.35 ± 0.01	904.2

phase equilibria, and are displayed graphically in Fig. 9. The insert refers to the assemblage olivine + rocksalt, the main figure to the assemblage spinel + rocksalt. If one assumes that at 800°C and 0.57 kbar, (NiMg)O still does not deviate markedly from ideality, then $\log C$ can be calculated similarly from the hydrothermal data, as also shown in Fig. 9. The maximum in $\log C$ in the spinel phase near $X_{NiGe_{0.5}O_2}$ appears to be real in both sets of data, although the error in $\log C$ increases sharply as either mole fraction approaches unity. Separate curves have been drawn to fit the 800 and the 1200°C data, although both sets of data could probably be equally well represented by one curve.

Three sets of calculations of activity–composition relations have been carried out using the smoothed $\log C$ vs X curves shown:

(a) The activity–composition relations at 1200°C were calculated using the actual phases, Mg_2GeO_4 (ol) and Ni_2GeO_4 (sp), as reference states. The results are shown in Table VI.

(b) At 1200°C, the hypothetical spinel form of Mg_2GeO_4 can be used as a reference state by extrapolating the $\log C$ vs X curve in the spinel in Fig. 9. Obviously this method introduces substantial uncertainties, but its results, shown in Table VI, can usefully be compared with those for 800°C, where the spinel solid solution series is continuous. Analogous extrapolations have been performed previously (*19*, *34*).

(c) At 800°C and 0.57 kbar, integration of Eqs. (4) and (5) is straightforward, since values of $\log C$ are experimentally accessible over the entire composition range. The spinels are the obvious reference states in these calculations.

The resulting activity–composition relations are shown in Figs. 10 and 11. All three plots have one feature in common: The activity of the nickel end-member initially deviates *negatively*

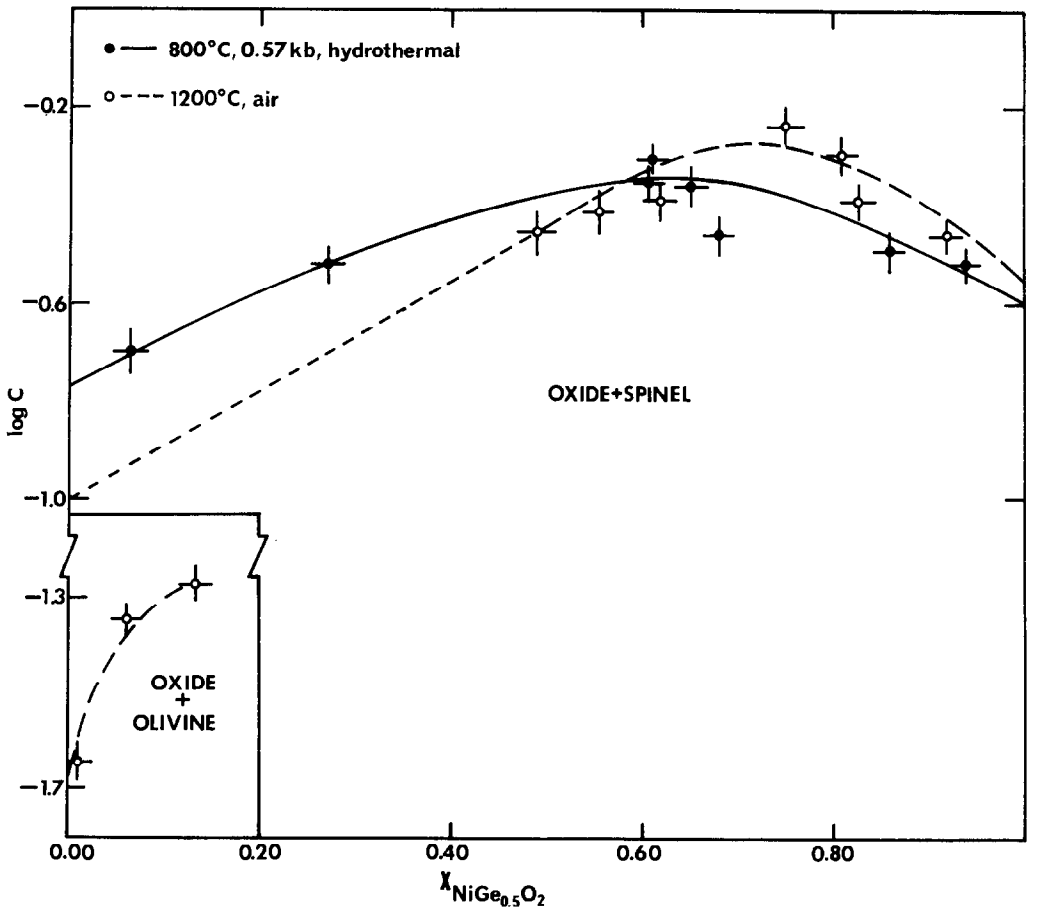

FIG. 9. Variation of $\log C$ with composition for orthogermanate plus oxide equilibria in system NiO–MgO–GeO_2.

TABLE VI

ACTIVITY COEFFICIENTS IN SYSTEM Ni_2GeO_4–Mg_2GeO_4 CALCULATED FROM ORTHOGERMANATE PLUS OXIDE EQUILIBRIUM

$X_{NiGe_{0.5}O_2}$	log C[a]	log $\gamma_{MgGe_{0.5}O_2}$	log $\gamma_{NiGe_{0.5}O_2}$	log K
$T = 1200°C, P = 1$ atm (air), actual solid solutions (ol + sp)				
0.00	(−1.68)[b]	0.00	(+0.61)	(−1.07)
0.05	−1.40	$+0.00_7$	+0.61	(−0.80)
0.10	−1.30	$+0.01_2$	+0.62	−0.69
0.13[c]	−1.27	$+0.01_5$	+0.62	−0.66
0.49_5[d]	−0.45	+0.25	+0.04	−0.66
0.55	−0.40	+0.28	+0.02	−0.66
0.60	−0.35	+0.31	±0.00	−0.66
0.65	−0.30	+0.34	−0.02	−0.66
0.70	−0.27	+0.36	−0.03	−0.66
0.75	−0.27	+0.36	−0.03	−0.66
0.80	−0.30	+0.34	−0.02	−0.66
0.85	−0.35	+0.29	−0.02	−0.66
0.90	−0.42	+0.24	-0.00_6	−0.66
0.95	−0.48	+0.18	-0.00_2	−0.66
1.00	(−0.54)[b]	+0.12	0.00_0	−0.66
$T = 1200°C, P = 1$ atm (air) extrapolated complete spinel solid solutions				
0.00	(−0.99)[b,e]	0.00	+0.46	0.53
0.10	(−0.89)[e]	0.00	+0.36	0.53
0.20	(−0.78)[e]	+0.01	+0.26	0.53
0.30	(−0.67)[e]	+0.03	+0.17	0.53
0.40	(−0.56)[e]	+0.07	+0.10	0.53
0.50	−0.45	+0.12	+0.04	0.53
0.60	−0.35	+0.18	±0.00	0.53
0.70	−0.27	+0.23	−0.03	0.53
0.80	−0.30	+0.21	−0.02	0.53
0.90	−0.42	+0.12	-0.00_6	0.53
1.00	(−0.54)[b]	+0.01	±0.000	0.53
$T = 800°C, P = 0.57$ kbar, hydrothermal runs, complete spinel solid solution				
0.00	(−0.77)[b]	0.00	(+0.26)	−0.51
0.10	−0.67	+0.01	+0.17	−0.51
0.20	−0.58	+0.02	+0.09	−0.51
0.30	−0.50	+0.05	+0.04	−0.51
0.40	−0.43	+0.07	−0.01	−0.51
0.50	−0.38	+0.10	−0.03	−0.51
0.60	−0.35	+0.12	−0.04	−0.51
0.70	−0.36	+0.11	−0.04	−0.51
0.80	−0.41	+0.08	−0.02	−0.51
0.90	−0.50	±0.00	−0.01	−0.51
1.00	(−0.56)[b]	−0.05	±0.00	−0.51

[a] Smoothed values of log C from Fig. 9.

[b] Values in parentheses are extrapolations to endpoints in Fig. 11.

[c] Boundary of olivine phase.

[d] Boundary of spinel phase.

[e] Linear extrapolation as shown in Fig. 11 for hypothetical complete spinel solid solution.

from ideality at high $X_{NiGe_{0.5}O_2}$. This mirrors the maximum in log C mentioned earlier, which exists at both 800 and 1200°C. Similar thermodynamic behavior has been observed for the spinel system Ni_2TiO_4–Zn_2TiO_4 at 1050°C (*34*), although there the spinel solid solution is unstable relative to (NiZn)O and (NiZn)TiO_3 at high ratios of Ni/Ni + Zn.

The two curves in Fig. 11 which refer to spinel standard states for both end-members agree fairly well with each other when one considers the uncertainties in the extrapolation at 1200°C. It is possible that the apparently complex deviation from ideality in the spinel orthogermanate solid solutions reflects in part an undetected deviation from ideality in (NiMg)O, especially at the lower temperature, but it seems doubtful that this could be the entire explanation, especially when one realizes that a_{NiO} in (NiMg)O can be gotten *most* accurately by reduction equilibrium studies on the *high* NiO portion of that system. Thus, our data suggest that the assumption that orthogermanate solid solutions behave ideally with respect to components of the same structure is *not* always strictly correct, and estimates of olivine–spinel stability relations based on this approximation are subject to some uncertainty.

It is interesting to seek a *structural* explanation for this behavior. One possibility is the aforementioned possibility of a changing cation distribution in the spinel solid solution series. Since Reinen's spectroscopic data seem to preclude the presence of any significant amounts of Ni^{2+} and Co^{2+} on tetrahedral sites (*12*), it would appear that only the colorless ions Mg^{2+} and Ge^{2+} can be involved in any octahedral–tetrahedral redistribution equilibria. For the Ni_2GeO_4–Mg_2GeO_4 series, one can satisfy this requirement by writing the substitution series:

$$\begin{aligned} Ge[Ni_2]O_4 &\rightarrow Mg_xGe_{1-x}[Ge_xNi_{2-x}]O_4 \\ &\rightarrow Mg[GeNi]O_4 \\ &\rightarrow Mg[GeMg_xNi_{1-x}]O_4 \\ &\rightarrow Mg[GeMg]O_4, \end{aligned} \qquad (6)$$

as the limiting case of a completely ordered substitution if Mg_2GeO_4 is indeed an inverse spinel. Two major objections can be raised against this. Firstly, with an ordered substitution of this sort, it is hard to rationalize the observed close adherence to Vegard's law across the entire composition range. Secondly, whereas such a

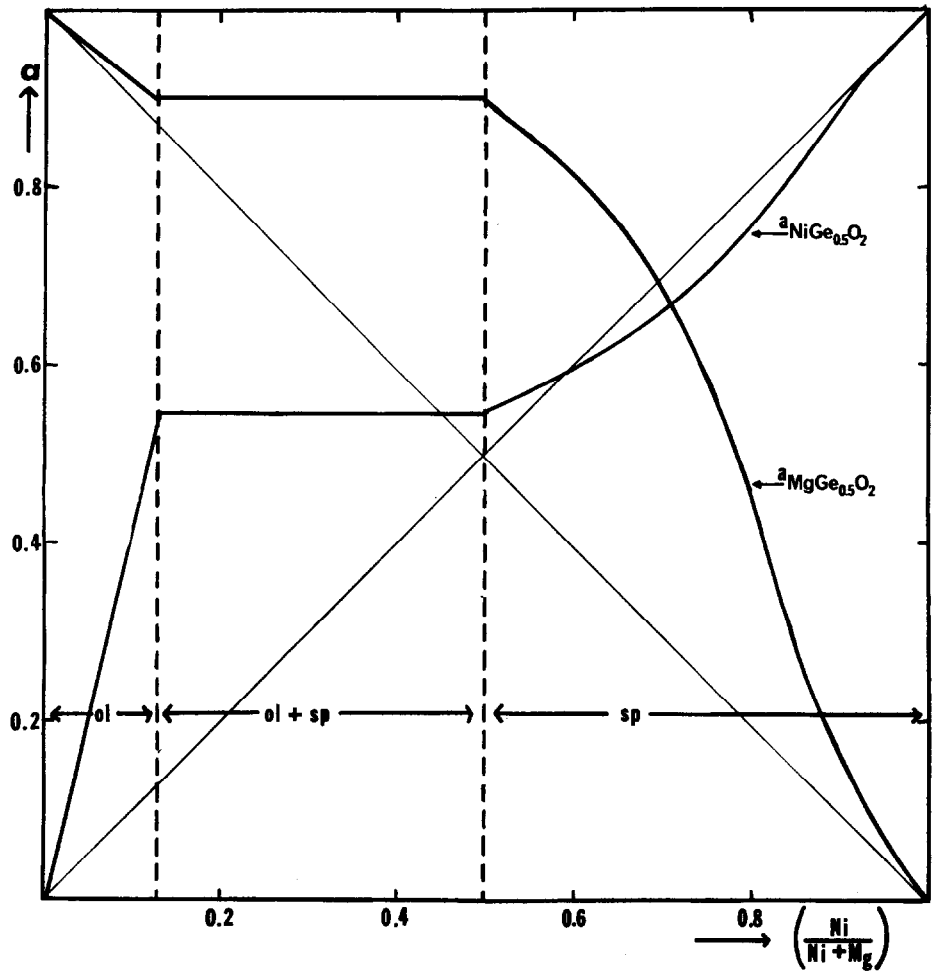

FIG. 10. Activity–composition relations along orthogermanate join in system NiO–MgO–GeO_2 at 1200°C in air.

sequence seems possible enough for the nickel-containing system, it is hard to see what factors would restrict all Co^{2+} to octahedral sites in the system Co_2GeO_4–Mg_2GeO_4 if an analogous substitution scheme applied. A possible way out of these difficulties lies in regarding Eq. (6) as a limiting scheme only, while in the real solutions only a small amount, perhaps on the order of 10%, of the tetrahedral Ge^{4+} is replaced by Mg^{2+}, which would lead to an Mg_2GeO_4 of somewhat disordered, rather than totally normal or totally inverse, cation distribution. This could account for complexities in the activity–composition relations without leading to the above difficulties. Obviously a detailed structural study of a single crystal of Mg_2GeO_4 spinel would help answer such questions.

An alternate structural rationalization of the thermodynamic data is feasible. Reinen (*12*, *39*) found that in the series Mg_2GeO_4–Ni_2GeO_4 and Mg_2GeO_4–Co_2GeO_4 the visible spectra show marked band splittings, which can be accounted for by a compression along the trigonal axes (oxygen parameter, $u = <0.375$) of the M^{2+}-containing octahedra. Although the magnitude of these splittings remains quite constant along each solid solution series, it seems possible that some subtleties in the overall energetics are affected by the substitution of Mg^{2+} for transition metal ions. In part, these may lead to short range ordering of the two divalent cations on octahedral sites or to some small changes in repulsion or crystal-field energies, which might account for the thermodynamics without invoking any disorder whatever on the tetrahedral sublattice.

In the system CoO–MgO–GeO_2, it is impossible to calculate orthogermanate activity–composition relations from the $(CoMg)_2GeO_4$–(CoMg)O

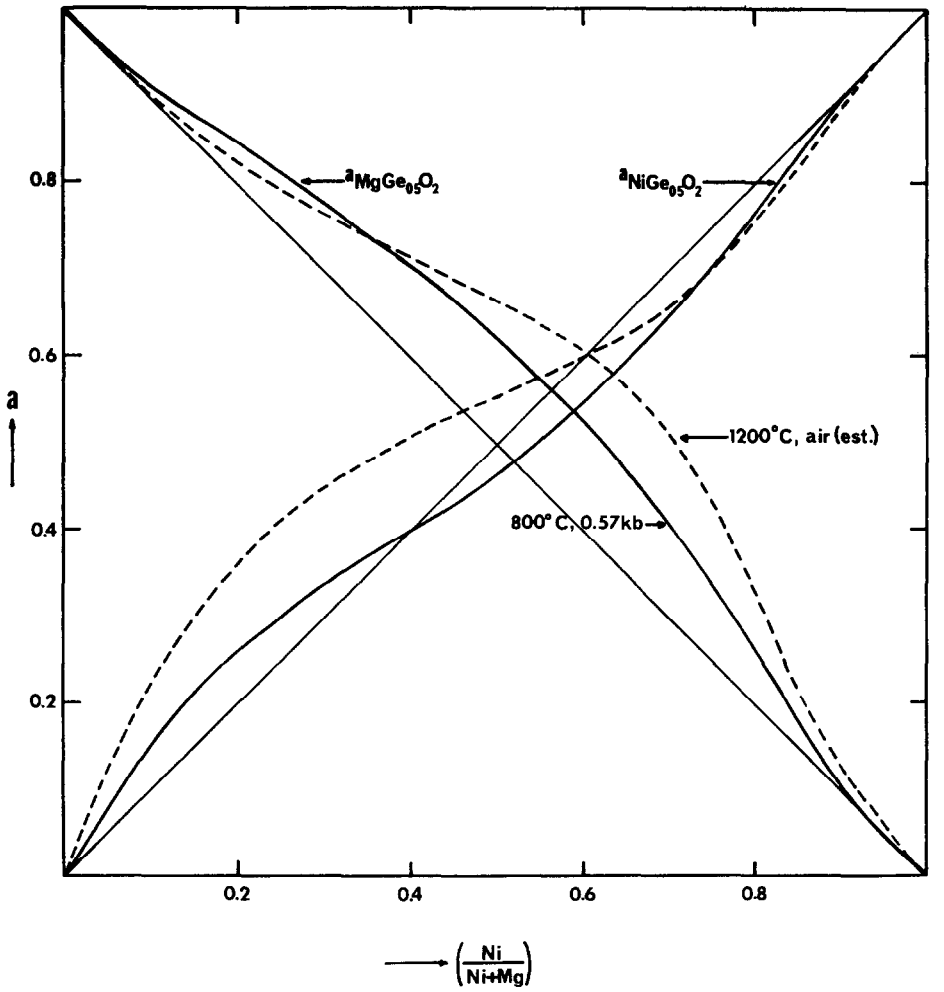

FIG. 11. Activity–composition relations in continuous spinel solid solutions $(NiMg)Ge_{0.5}O_2$.

equilibrium because of the existence of a compound or series of compounds near $X_{GeO_2} = 0.24$. The following approach was taken instead. The enstatite solid solution across the metagermanate join is continuous. In the corresponding silicate system, the orthopyroxene $(CoMg)SiO_3$ solid solution shows virtually no deviations from Vegard's law, in contrast to the $(NiMg)SiO_3$ and $(FeMg)SiO_3$ systems (*40*). This would be consistent with very little ordering of Co^{2+} and Mg^{2+} on the M_1 and M_2 sites in the pyroxene structure (*40*). Our lattice parameter data for the system $(CoMg)GeO_3$, though not very precise, show a virtually linear variation of lattice parameters with composition. The apparent absence of cation ordering and the similar sizes of Co^{2+} and Mg^{2+} suggest that deviations from thermodynamic ideality in $(CoMg)SiO_3$ and also in $(CoMg)GeO_3$ are probably quite small. Though the CoO–MgO–SiO_2 system has not been studied thermodynamically, $(CoMn)SiO_3$ has been found to be ideal (*41*), as has $(CoMg)Al_2O$ (*42*), while $(CoMg)TiO_3$ shows very small negative deviations from ideality (*43*).

Thus the ideality of $(CoMg)GeO_3$ solid solutions is a reasonable first approximation. On that basis, activity–composition relations on the $(CoMg)_2GeO_4$ join can be estimated. One can write the equilibrium:

$$(MgGeO_3)_{ss} + (CoGe_{0.5}O_2)_{ss} = (CoGeO_3)_{ss} + (MgGe_{0.5}O_2)_{ss}, \quad (7)$$

for which

$$\log K = \log C + \log \gamma_{MgGe_{0.5}O_2} - \log \gamma_{CoGe_{0.5}O_2}, \quad (8)$$

where

$$C = \frac{a_{CoGeO_3} X_{MgGe_{0.5}O_2}}{a_{MgGeO_3} X_{CoGe_{0.5}O_2}} \approx \frac{X_{CoGeO_3} X_{MgGe_{0.5}O_2}}{X_{MgGeO_3} X_{CoGe_{0.5}O_2}}. \quad (9)$$

Calculated values of $\log C$ in the spinel plus pyroxene field (compositions of the spinel phase obtained from its lattice parameters, which give the conjugation lines in Fig. 8) are shown in Table VII. These values show a good deal of scatter, and no trend in $\log C$ vs $X_{CoGe_{0.5}O_2}$ is apparent. In view of the approximations on which this calculation is based, it seems best to assume $\log C$ is roughly constant in the spinel phase. Then $\gamma_{CoGe_{0.5}O_2} = 1$ and $\gamma_{MgGe_{0.5}O_2}$ is constant therein. Similarly, for lack of more detailed information in the olivine phase, we must assume that $\gamma_{MgGe_{0.5}O_2} = 1$ and $\gamma_{CoGe_{0.5}O_2}$ is constant therein. We then have:

$$\gamma_{MgGe_{0.5}O_2}\,(\text{spinel}) = \frac{a_{MgGe_{0.5}O_2}\,(\text{two phase})}{X_{MgGe_{0.5}O_2}\,(\text{terminal spinel})} \approx \frac{X_{MgGe_{0.5}O_2}\,(\text{terminal olivine})}{X_{MgGe_{0.5}O_2}\,(\text{terminal spinel})}, \quad (10)$$

and similarly:

$$\gamma_{CoGe_{0.5}O_2}\,(\text{olivine}) \approx \frac{X_{CoGe_{0.5}O_2}\,(\text{terminal olivine})}{X_{CoGe_{0.5}O_2}\,(\text{terminal spinel})}. \quad (11)$$

The results of these calculations are shown in Table VII and the approximate activity–composition relations are exhibited in Fig. 12.

Free Energies of Transformation Between Olivine and Spinel Structures for Mg_2GeO_4, Ni_2GeO_4, and Co_2GeO_4

Three independent means can be used to estimate the free energy of transformation of Mg_2GeO_4 from the olivine to the spinel structure at 1200°C and atmospheric pressure. From the study by Dachille and Roy (*7*), the Clausius–Clapeyron slope for the transition gives, at 810°C, $\Delta H^\circ = -3.69$ kcal/mole, and $\Delta S^\circ = -3.4$ cal/degree mole. Neglecting the variation of ΔH° and ΔS° with temperature, we have, for the reaction

$$Mg_2GeO_4\ (\text{ol}) = Mg_2GeO_4\ (\text{sp}), \quad (12)$$

$$\Delta G^\circ_{1473} = \Delta H^\circ - T\Delta S^\circ = +1.3 \text{ kcal/mole}. \quad (13)$$

Secondly, we have calculated activity–composition relations in the system $(MgNi)_2GeO_4$ at 1200°C both with the olivine as standard state and with the hypothetical spinel as standard state. It follows from Eqs. (2) and (3) that

$$-2.3\,RT\log K = \tfrac{1}{2}(\Delta G^\circ_{Ni_2GeO_4} - \Delta G^\circ_{Mg_2GeO_4}), \quad (14)$$

where $\Delta G^\circ_{Ni_2GeO_4}$ and $\Delta G^\circ_{Mg_2GeO_4}$ are the standard free energies of formation from the oxides of the germanates in the structures used as standard states. From Table VI, we then have, at 1200°C,

$$2.3\,RT(0.66) = \tfrac{1}{2}(\Delta G^\circ_{Ni_2GeO_4\,(sp)} - \Delta G^\circ_{Mg_2GeO_4\,(ol)}), \quad (15)$$

and

$$2.3\,RT(0.53) = \tfrac{1}{2}(\Delta G^\circ_{Ni_2GeO_4\,(sp)} - \Delta G^\circ_{Mg_2GeO_4\,(sp)}); \quad (16)$$

TABLE VII

APPROXIMATE ACTIVITY–COMPOSITION RELATIONS ON ORTHOGERMANATE JOIN FROM $(CoMg)GeO_3$–$(CoMg)_2GeO_4$ EQUILIBRIUM IN SYSTEM CoO–MgO–GeO_2 AT 1200°C

$X_{CoGe_{0.5}O_2}$	Phases	C[a]	$\log C$	$\log \gamma_{MgGe_{0.5}O_2}$	$\log \gamma_{CoGe_{0.5}O_2}$	$\log K$
0.225[b]	ol + sp + py	1.06	+0.02	0	0.26	−0.24
0.410[c]	ol + sp + py	0.442	−0.35			
0.605	sp + py	0.666	−0.18			
0.767	sp + py	0.416	−0.38			
0.800	sp + py	0.464	−0.33			
0.850	sp + py	0.591	−0.23			
0.955	sp + py	0.424	−0.37			
		Av. (sp) =	−0.31	0.12	0	−0.19

[a] From Eq. (8).
[b] Terminal olivine composition Fig. 11.
[c] Terminal spinel composition Fig. 11.

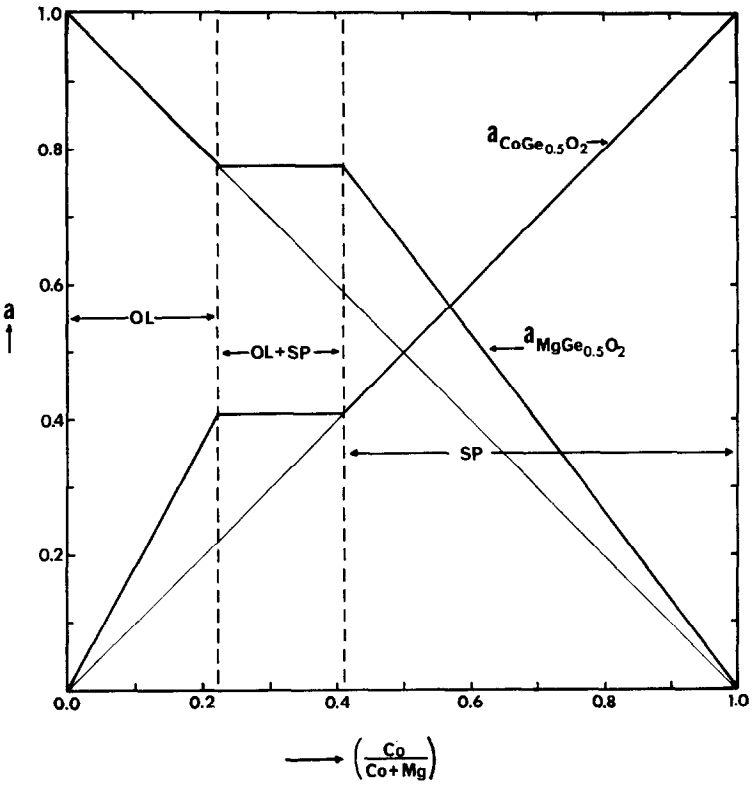

FIG. 12. Activity–composition relations along orthogermanate join in system CoO–MgO–GeO_2 at 1200°C in air.

or

$$2.3\,RT(0.13) = \tfrac{1}{2}(\Delta G^\circ_{Mg_2GeO_4\,(sp)} - \Delta G^\circ_{Mg_2GeO_4\,(ol)}), \quad (17)$$

and

$$\Delta G^\circ_{Mg_2GeO_4\,(sp)} - \Delta G^\circ_{Mg_2GeO_4\,(ol)} = 1.7 \text{ kcal/mole}. \quad (18)$$

Lastly, the limiting activity coefficients of Mg_2GeO_4 (ol) in the spinel phase can be used to estimate its free energy of transformation to that structure (*20*, *21*).

$$\Delta G^\circ_{12} = 2 \times 2.3\,RT \log \gamma^\circ_{MgGe_{0.5}O_2}. \quad (19)$$

The limiting values of $\log \gamma_{MgGe_{0.5}O_2}$ are +0.12 from the system NiO–MgO–GeO_2, and also approx 0.12 from CoO–MgO–GeO_2, so ΔG°_{12} = 1.6 kcal/mole.

Thus the three estimates yield 1.3, 1.7, and 1.6 kcal/mole for the free energy of the olivine–spinel transition in Mg_2GeO_4 at 1200°C. This consistency lends support to the validity of the approach used in the present work.

For the olivine–spinel transition in Ni_2GeO_4 and Co_2GeO_4, we can calculate the free energy of transformation from the limiting activity coefficients in the olivine phase ($\log \gamma^\circ = 0.61$ and 0.26, respectively). For the reaction:

$$Ni_2GeO_4 \text{ (ol)} \rightarrow Ni_2GeO_4 \text{ (sp)}, \quad (20)$$

$$\Delta G^\circ = -2 \times 2.3\,RT \log \gamma^\circ_{NiGe_{0.5}O_2} = -8.2 \text{ kcal/mole}; \quad (21)$$

while for

$$Co_2GeO_4 \text{ (ol)} \rightarrow Co_2GeO_4 \text{ (sp)}, \quad (22)$$

$$\Delta G^\circ = -2 \times 2.3\,RT \log \gamma^\circ_{CoGe_{0.5}O_2} = -3.5 \text{ kcal/mole}. \quad (23)$$

Thus the relative stability of the spinel structure with respect to the olivine increases in the series Mg < Co < Ni in both the germanates studied here and in the silicates (*26*). Further discussion of such trends is reserved for a later paper in this series, which can draw upon experimental data for these and other systems.

Free Energies of Formation of Germanates

Calculations like those above from conjugation lines in ternary systems have been used successfully to estimate the free energies of formation of end-member silicates such as

Mg_2SiO_4 and $MgSiO_3$ from equilibria in ternary systems such as MgO–FeO–SiO_2 when the free energies of formation of the other end-members, such as Fe_2SiO_4, are known (*19*). The difficulty in applying this method to the germanates arises from the unavailability of independently determined free energy values for any end-member. The usual techniques of gas equilibration and solid cell emf fail for the transition-metal germanates because GeO_2 is reduced to Ge metal at oxygen pressures only slightly below the Co–CoO equilibrium (*44*). Because Ge metal has a low melting point and a high vapor pressure (*44*), loss of germanium from germanate samples begins to be substantial even at moderately high oxygen pressures, as mentioned above. The possible existence of GeO and of transition metal–germanium alloys further complicates the picture. It may be feasible to determine the free energy of formation of noble metal germanates (Mg_2GeO_4, $MgGeO_3$) by reduction equilibria involving Ge metal or its vapor, but at present no data are available.

However, the present investigation does provide values for the differences in free energies of formation $\Delta(\Delta G^\circ)$ between pairs of germanate end-members. These can be compared with the available calorimetrically determined values of enthalpy differences, $\Delta(\Delta H^\circ)$ (*15*).

From the orthogermanate plus oxide equilibrium in the system NiO–MgO–GeO_2, and Eq. (15), we have

$$\Delta G^\circ_{Ni_2GeO_4\,(sp)} - \Delta G^\circ_{Mg_2GeO_4\,(ol)} = \Delta(\Delta G^\circ) = +8.9 \text{ kcal}, \quad (24)$$

and, from calorimetric heats of formation,

$$\Delta(\Delta H^\circ) = +12.4 \text{ kcal}. \quad (25)$$

The pyroxene solid solution in the system NiO–MgO–GeO_2 extends only to $X_{NiGeO_3} = 0.135$. We can write the equilibrium

$$(MgGeO_3)_{ss} + (NiGe_{0.5}O_2)_{ss} = (NiGeO_3)_{ss} + (MgGe_{0.5}O_2)_{ss}, \quad (26)$$

for which

$$\log C = \log(X_{NiGeO_3} a_{MgGe_{0.5}O_2} / X_{MgGeO_3} a_{NiGe_{0.5}O_2}). \quad (27)$$

We can calculate $\log C$ at two points. Pyroxene of $X_{NiGeO_3} = \sim 0.07$ (see Fig. 6) coexists with olivine plus spinel, where $a_{MgGe_{0.5}O_2} = 0.55$ and $a_{NiGe_{0.5}O_2} = 0.90$, so that $\log C = -0.95$. At the termination of the (NiMg)GeO_3-phase, pyroxene with $X_{NiGeO_3} = 0.135$ coexists with spinel of $X_{Ni_2GeO_4} = 0.815$ and a melt that is probably fairly close to pure GeO_2 in composition. Log C for this assemblage is -1.09.

These two values are quite similar, and if one neglects deviations from ideality in the pyroxene solid solution, then $\log C \approx \log K$, and

$$-2.3\,RT \log K = \Delta G^\circ_{NiGeO_3} - \Delta G^\circ_{MgGeO_3} + \tfrac{1}{2}(\Delta G^\circ_{Mg_2GeO_4} - \Delta G^\circ_{Ni_2GeO_4}). \quad (28)$$

Substituting the values from Eq. (25) and -1.0_2 as the average value of $\log K$, we get

$$\Delta G^\circ_{NiGeO_3} - \Delta G^\circ_{MgGeO_3} = +11.7 \text{ kcal}. \quad (29)$$

This large difference is consistent with the instability of $NiGeO_3$ and the small extent of the pyroxene solid solution.

For the CoO–MgO–GeO_2 system (see Table VII), we get, from Eqs. (7) and (8), $\log K = -0.2$ and

$$\Delta G^\circ_{CoGeO_3} - \Delta G^\circ_{MgGeO_3} + \tfrac{1}{2}(\Delta G^\circ_{Mg_2GeO_4} - \Delta G^\circ_{Co_2GeO_4}) = \Delta(\Delta G^\circ) = +1.3 \text{ kcal}. \quad (30)$$

For the same reactions, $\Delta(\Delta H^\circ) = +2.5$ kcal from calorimetric measurements (*15*).

These free energy data are not very precise (probably $\pm 10\%$), but they compare reasonably with the calorimetric data. Both show that stability decreases in the sequences Mg_2GeO_4, Co_2GeO_4, Ni_2GeO_4, and $MgGeO_3$, $CoGeO_3$, $NiGeO_3$, with the last compound unstable relative to Ni_2GeO_4 and GeO_2. Also, the calculated differences in entropies of formation,

$$\Delta(\Delta S^\circ) = [\Delta(\Delta H^\circ) - \Delta(\Delta G^\circ)]/T, \quad (31)$$

would be not larger in magnitude than 3 cal/°C for any of these assemblages, which is reasonable for pairs of condensed phases of similar structures.

Acknowledgments

I thank the National Science Foundation (Grant GP 20402) and the Research Corporation for support of this work. The germanium dioxide used was generously provided by the Sylvania Corporation.

References

1. V. M. GOLDSCHMIDT, *Nachr. Ges. Wiss. Goettingen Math. Phys. Kl.* **2**, 184 (1931).
2. A. E. RINGWOOD, *in* "Advances in Earth Science" (P. M. Hurley, Ed.), pp. 373–388. M.I.T. Press, Cambridge, MA, 1964.

3. A. E. RINGWOOD, *Phys. Earth Planet Interiors* **3**, 109 (1970).
4. Y. SYONO, S. AKIMOTO, AND Y. MATSUI, *J. Solid State Chem.* **3**, 369 (1971).
5. C. J. M. ROOYMANS, *Philips Res. Rep. Suppl.* No. 5 (1968).
6. A. E. RINGWOOD AND A. MAJOR, *Nature (London)* **215**, 1367 (1967).
7. F. DACHILLE AND R. ROY, *Amer. J. Sci.* **258**, 225 (1960).
8. J. D. BERNAL, *Observatory* **59**, 268 (1936).
9. S. AKIMOTO AND Y. SATO, Technical Report No. 328, Institute of Solid State Physics, University of Tokyo, Series A (1968).
10. A. E. RINGWOOD AND A. MAJOR, *Phys. Earth Planet Interiors* **3**, 89 (1970).
11. B. KAMB, *Amer. Mineral.* **53**, 1439 (1968).
12. D. REINEN, *Z. Anorg. Allg. Chem.* **356**, 182 (1968).
13. Y. SYONO, *Phys. Earth Planet. Interiors* (in press).
14. R. C. EVANS, "An Introduction to Crystal Chemistry," 2nd ed., pp. 140, 242. Cambridge University Press, London, 1966.
15. A. NAVROTSKY, *J. Inorg. Nucl. Chem.* **33**, 4035 (1971).
16. S. AKIMOTO AND H. FUJISAWA, *J. Geophys. Res.* **73**, 1467 (1968).
17. S. AKIMOTO, H. FUJISAWA, AND T. KATSURA, *J. Geophys. Res.* **70**, 1969 (1965).
18. A. E. RINGWOOD, *Geochim. Cosmochim. Acta* **15**, 18 (1958).
19. A. MUAN, *Proc. Brit. Ceram. Soc.* **8**, 103 (1967).
20. C. LANDOLT AND A. MUAN, *J. Inorg. Nucl. Chem.* **31**, 1319 (1969).
21. A. NAVROTSKY AND A. MUAN, *J. Inorg. Nucl. Chem.* **33**, 35 (1971).
22. D. S. KENNY AND A. NAVROTSKY, *J. Inorg. Nucl. Chem.* (in press).
23. E. J. W. WHITTAKER AND R. MUNTUS, *Geochim. Cosmochim. Acta* **34**, 945 (1970).
24. A. D. WADSLEY, A. F. REID, AND A. E. RINGWOOD, *Acta Crystallogr. Sect. B* **24**, 740 (1968).
25. C. R. ROBBINS AND E. M. LEVIN, *Amer. J. Sci.* **257**, 63 (1959).
26. E. KOSTINER AND P. W. BLESS, *J. Electrochem. Soc.* **118**, 351 (1971).
27. P. ROYEN AND W. FORWERG, *Z. Anorg. Allgem. Chem.* **326**, 113 (1963).
28. R. ROMEIJN, *Philips Res. Rep.* **8**, 304 (1953).
29. A. TAUBER AND J. A. KOHN, *Amer. Mineral.* **50**, 13 (1965).
30. A. E. RINGWOOD, *Geochim. Cosmochim. Acta* **26**, 459 (1962).
31. A. E. RINGWOOD, *Aust. J. Sci.*, 378 (1961).
32. R. K. DATTA AND R. ROY, *Z. Kristallogr.* **121**, 416 (1965).
33. A. NAVROTSKY, *J. Inorg. Nucl. Chem.* **31**, 59 (1969).
34. A. NAVROTSKY AND A. MUAN, *J. Inorg. Nucl. Chem.* **32**, 3471 (1970).
35. A. W. LAUBENGAYER AND D. S. MORTON, *J. Amer. Chem. Soc.* **54**, 2303 (1932).
36. E. AUKRUST AND A. MUAN, *Trans. Met. Soc. AIME* **227**, 1378 (1963).
37. W. C. HAHN AND A. MUAN, *J. Phys. Chem. Solids* **19**, 338 (1961).
38. C. PETOT, G. PETOT-ERVAS, AND M. RIGUAD, *Can. Met. Quart.* **10**, 203 (1971).
39. D. REINEN, *Theor. Chim. Acta* **8**, 260 (1967).
40. Y. MATSUI, Y. SYONO, S. AKIMOTO, AND K. KITAYAMA, *Geochem. J.* **2**, 61 (1968).
41. J. V. BIGGERS AND A. MUAN, *J. Amer. Ceram. Soc.* **50**, 230 (1967).
42. E. ROSEN AND A. MUAN, *J. Amer. Ceram. Soc.* **49**, 107 (1966).
43. B. BREZNY AND A. MUAN, *Thermochim. Acta* **2**, 107 (1971).
44. R. A. ROBIE AND D. R. WALDBAUM, U.S. Geol. Survey Bulletin No. 1259, 1968.